# Dielectric screening effects on electron transport in Ga0.51In0.49P/InxGa1−xAs/GaAs quantum wells

C. Besikci, A. T. Bakir, and B. Tanatar

Citation: J. Appl. Phys. **88**, 1504 (2000); doi: 10.1063/1.373846
View online: http://dx.doi.org/10.1063/1.373846
View Table of Contents: http://jap.aip.org/resource/1/JAPIAU/v88/i3
Published by the American Institute of Physics.

# Dielectric screening effects on electron transport in $Ga_{0.51}In_{0.49}P/In_xGa_{1-x}As/GaAs$ quantum wells

C. Besikci[a] and A. T. Bakir
*Electrical Engineering Department, Middle East Technical University, 06531 Ankara, Turkey*

B. Tanatar
*Department of Physics, Bilkent University, 06533 Ankara, Turkey*

(Received 13 December 1999; accepted for publication 18 April 2000)

The effects of dielectric screening on the two dimensional polar optical phonon scattering and on electron transport in $Ga_{0.51}In_{0.49}P/In_xGa_{1-x}As/GaAs$ ($x=0$, 0.15, and 0.25) modulation doped heterostructures and high electron mobility transistors are investigated through the ensemble Monte Carlo technique. The two dimensional polar optical phonon scattering rates including and excluding dielectric screening effects are calculated using the self-consistently evaluated electronic states in the quantum well. The calculated scattering rates are compared in order to see the effects of screening on the inter- and intra-subband scattering. Screening significantly lowers the intra-subband polar optical phonon scattering rates in both lattice matched and pseudomorphic structures. This results in a considerable lowering of the critical electric field beyond which negative differential resistance is seen. Screening also modifies the dependence of transport properties on the quantum well parameters. The results of the ensemble Monte Carlo simulations of high electron mobility transistors show that the performance of the device is considerably underestimated, if screening is not included in the calculation of the polar optical phonon scattering rates. © *2000 American Institute of Physics.* [S0021-8979(00)00515-6]

## I. INTRODUCTION

III–V heterostructures have widely been used for high performance electron devices such as high electron mobility transistor (HEMT) and optical devices such as quantum well photodetectors and lasers. AlGaAs is the most commonly used large band gap material for heterostructure devices on GaAs substrates. However, due to the well known advantages of GaInP over AlGaAs,[1] this material has recently received increasing attention to replace AlGaAs,[2–6] and high performance $Ga_{0.51}In_{0.49}P/In_xGa_{1-x}As/GaAs$ HEMTs have been demonstrated.

In order to use the desirable transport properties of the two dimensional electron gas (2DEG) efficiently in quantum well devices such as HEMTs, one must have a sound understanding of the physics of carrier transport in 2D systems. Phonon, impurity, and alloy scattering mechanisms in 2DEG have been studied[7–12] and the 2DEG velocity-field characteristics in modulation doped heterostructures have been investigated through Monte Carlo simulations.[13–16] There have been many efforts to develop an accurate model for HEMTs. A review of these models was presented by Salmer *et al.*[17] The Monte Carlo technique has been the most accurate and complete method for the simulation and optimization of HEMTs.[18–20] However, some mechanisms, which are assumed to be of second order, such as screening in polar optical phonon (POP) scattering, were ignored in the previous device simulations. Screened electron–polar optical phonon interaction has been investigated by Price[21] and Basu and Kundu.[22] In this article, we present the results of precise Monte Carlo simulations of 2D electron transport in $Ga_{0.51}In_{0.49}P/In_xGa_{1-x}As/GaAs$ modulation doped structures and in HEMTs including the effects of dielectric screening in order to show the importance of screening effects. While the simulations performed in this work are for the $Ga_{0.51}In_{0.49}P/In_xGa_{1-x}As/GaAs$ heterostructures, main conclusions of the article should also be valid for modulation doped structures based on other material systems.

Our Monte Carlo simulation programs consider the lowest three subbands in the quantum well, $\Gamma$, $L$, and $X$ valleys of the conduction band and all the dominant 2D and 3D scattering mechanisms. In order to increase the accuracy of the results, trial subband wave functions are not used and the electronic states in the quantum well are calculated self-consistently by coupling the Schrödinger and Poisson's equations. Two dimensional scattering rates are calculated using the obtained results for the electronic states. The results of our work clearly show that POP screening should be taken into account in device Monte Carlo simulations in order to predict the dc and high frequency performance of the device correctly.

The procedure for calculating the quantum well electronic states is briefly presented in Sec. II. Section III describes the calculation of the 2D POP scattering rates including the dielectric screening effects and discusses the effects of screening on the inter- and intra-subband POP scattering. Effects of screening on the transport properties of the heterostructures are given in Sec. IV. Section V presents the results of HEMT ensemble Monte Carlo simulations and investigates the effects of screening on the device performance pre-

[a]Electronic mail: besikci@ed.eee.metu.edu.tr

 

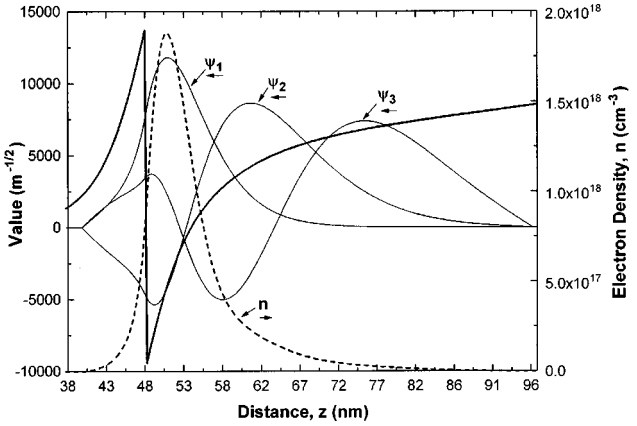


FIG. 1. 77 K wave functions in the $Ga_{0.51}In_{0.49}P/GaAs$ structure with a barrier layer doping of $2\times10^{18}\,cm^{-3}$. Energy levels for the lowest three subbands are 88, 130, and 146 meV, respectively.

dicted by the simulations. Concluding remarks are given in Sec. VI.

## II. QUANTUM WELL ELECTRONIC STATES

The electronic states in the $Ga_{0.51}In_{0.49}P/In_xGa_{1-x}As/GaAs$ modulation doped heterostructures with various channel In mole fraction ($x$), InGaAs layer thickness and barrier (GaInP) layer doping are calculated self-consistently by solving the Schrödinger equation using the Numerov method.[23] Assuming that the wave function parallel to the heterointerface ($xy$ plane) is in the form of a plane wave, Schrödinger equation for the envelope wave function for subband $m$ $[\Psi_m(z)]$ normal to the heterointerface can be expressed as

$$-\frac{\hbar^2}{2m^*}\frac{d^2\Psi_m(z)}{dz^2}+V(z)\Psi_m(z)=E_m\Psi_m(z), \tag{1}$$

where $V(z)$ is the effective potential.[24] When the lowest three subbands in the quantum well are taken into account, Poisson's equation in the quantum well reads

$$\frac{d^2U(z)}{dz^2}=\frac{e}{\epsilon}\left[\sum_{i=1}^{3} n_i\Psi_i^2(z)-N_D(z)+N_A(z)\right], \tag{2}$$

where $U(z)$ is the electrostatic potential, $N_D(z)$ is the ionized donor density, $N_A(z)$ is the ionized acceptor density, and $n_i$ is the density of electrons in subband $i$ found from

$$n_i=\frac{m^*kT}{\pi\hbar^2}\ln\left[1+\exp\left[\frac{E_F-E_i}{kT}\right]\right]. \tag{3}$$

The coupled Eqs. (1)–(3) are solved using the Numerov method. The Fermi–Dirac integral is also solved in degenerate regions of the heterostructures in order to establish a relation between the electron density and the Fermi level. A self-consistent solution procedure is carried out along 1500 mesh points distributed throughout the heterostructure.

Figure 1 shows the calculated subband wave functions at 77 K for the lattice matched GaInP/GaAs heterostructure with a GaInP (barrier) layer donor doping of $2\times10^{18}\,cm^{-3}$. The energy levels at this temperature are found to be 88, 130, and 146 meV, respectively for the lowest three subbands.

## III. 2D POLAR OPTICAL PHONON SCATTERING RATES

For a three-subband model, the polar optical phonon scattering rates are calculated using the Fermi's Golden Rule[7,25]

$$\Gamma_{ij}(k)=\frac{e^2w_{LO}}{2}\left(n_B(w_{LO})+\frac{1}{2}\mp\frac{1}{2}\right)\times\int d^2q\,\frac{H^{eff}_{jiij}(q)}{q}\,\delta[E_i(k)\mp\hbar w_{LO}-E_j(k\mp q)], \tag{4}$$

where the upper and lower signs refer to the emission and absorption processes, respectively. $n_B(w_{LO})$ is the Bose distribution function giving the average number of phonons with energy $\hbar w_{LO}$ at temperature $T$. Dielectric screening effects are taken into account within a static approximation by considering an effective interaction $H^{eff}$ defined in terms of the dielectric matrix[25]

$$H_{ijkl}(q)=\sum_{mn}\epsilon_{ijnm}(q,w=0)H^{eff}_{mnkl}(q). \tag{5}$$

In the absence of screening, the subband form factors are expressed by

$$H_{ijkl}(q)=\int_0^\infty dz\int_0^\infty dz'\,e^{-q|z-z'|}\Psi_i(z')\Psi_j(z')\Psi_k(z)\Psi_l(z) \tag{6}$$

in which the self-consistently calculated wave functions are used. The dielectric matrix embodying the screening effects is given in the random phase approximation by

$$\epsilon_{ijnm}(q)=\delta_{im}\delta_{jn}-V_{ijnm}(q)\chi_{nm}(q), \tag{7}$$

where $\chi_{nm}(q)$ is the static polarizability. The form factors and the Coulomb interaction matrix elements are related by $H_{ijkl}(q)=V_{ijkl}(q)/(2\pi e^2/q)$. In this work, we consider only the static dielectric function. The dynamical effects[25] worthy of a separate study are beyond the scope of the present calculation. The matrix elements of the static dielectric function $\epsilon(q)$ are calculated by keeping the full temperature dependence. The usual Thomas–Fermi screening corresponds to the $q\to0$ limit of our dielectric function. The static screening approximation adopted here should be appropriate for large carrier densities, since $\hbar w_{LO}$ remains small compared with the characteristic energy (i.e., plasmon energy) of the electron gas. The typical sheet electron densities in these heterostructures are usually larger than $1\times10^{12}\,cm^{-2}$ for electron device applications. In all the structures investigated in this work, two dimensional electron density is higher than this value.

In the calculation of the 2D scattering rates in the heterostructure quantum wells, approximate wave functions are commonly used. A single modulation doped heterostructure is usually approximated by a simple triangular quantum well and trial wave functions are used.[26] However, this approach may result in a large error in the calculated 2D scattering rates. In order to investigate the error introduced by this approach, we compared the 2D polar optical phonon scattering

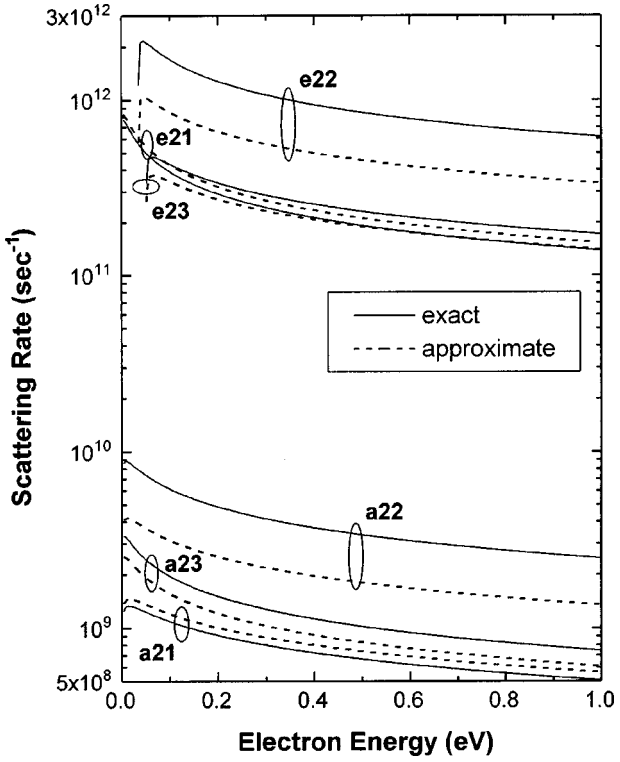


FIG. 2. 2D POP scattering rates in the second subband of the $Ga_{0.51}In_{0.49}P/GaAs$ structure with a barrier layer doping of $2\times10^{18}\,cm^{-3}$ calculated using the exact and trial wave functions at 77 K. $e_{ij}$ and $a_{ij}$ represent the emission and absorption rates from subband $i$ to $j$, respectively.

rates obtained using trial wave functions with those calculated by the exact wave functions. The exact wave functions were calculated self-consistently in the $Ga_{0.51}In_{0.49}P/GaAs$ single quantum well with $Ga_{0.51}In_{0.49}P$ layer donor doping of $2\times10^{18}\,cm^{-3}$. For comparison, we used the following trial wave functions based on a variational approach:

$$\phi_1(z)=(b^3/2)^{1/2}z\exp(-bz/2), \tag{8}$$

$$\phi_2(z)=(3b^3/2)^{1/2}z(1-bz/3)\exp(-bz/2), \tag{9}$$

$$\phi_3(z)=(3b^3)^{1/2}z(1-2bz/3+b^2z^2/12)\exp(-bz/2), \tag{10}$$

where the parameter $b=(33m^*e^2N_s/\epsilon_0)^{1/3}$ is related to the sheet electron density, $N_s$. Figure 2 shows the 2D polar optical phonon emission and absorption rates in the second subband. Especially the intrasubband scattering rates in this subband are greatly underestimated, if the trial wave functions are used. Therefore, we used the self-consistently calculated wave functions to obtain reasonable accuracy in the calculation of the transport in the heterostructures investigated in this work.

In order to see the effects of screening on POP scattering, we calculated two-dimensional POP scattering rates for both screened and unscreened cases. Figure 3 shows the POP emission and absorption rates at 77 K for the pseudomorphic $Ga_{0.51}In_{0.49}P/In_{0.15}Ga_{0.85}As/GaAs$ structure with an $In_{0.15}Ga_{0.85}As$ layer thickness of 10 nm and a $Ga_{0.51}In_{0.49}P$

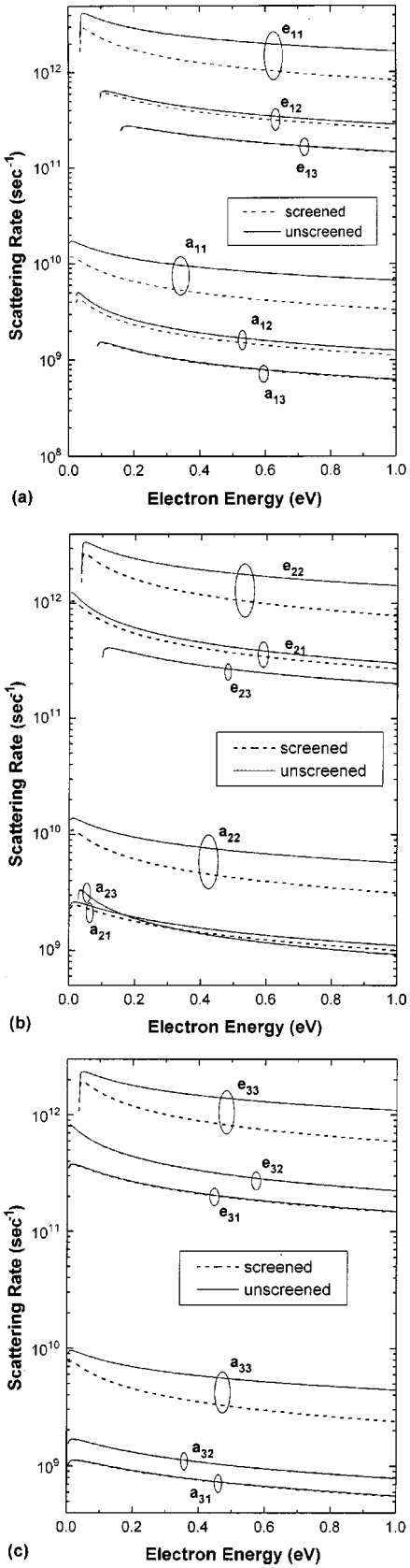


FIG. 3. 2D POP scattering rates in the $Ga_{0.51}In_{0.49}P/In_{0.15}Ga_{0.85}As/GaAs$ structure with a barrier layer doping of $2\times10^{18}\,cm^{-3}$ at 77 K. $e_{ij}$ and $a_{ij}$ represent the emission and absorption rates from subband $i$ to $j$, respectively. InGaAs layer thickness is 10 nm. First subband (a), second subband (b), and third subband (c).

layer doping of $2\times10^{18}\,\mathrm{cm}^{-3}$. The intrasubband POP scattering rate is significantly lowered due to dielectric screening, whereas the intersubband rates are almost unaffected. This is mainly due to the rapidly decreasing strength of the intersubband Coulomb matrix elements, $H_{ijkl}(q)$. Similar differences between screened and unscreened POP rates were seen in our calculations for single well modulation doped $Ga_{0.51}In_{0.49}P$/GaAs structures.

## IV. EFFECTS OF SCREENING ON TRANSPORT PROPERTIES

In order to see the effects of screening on the two-dimensional electron gas transport, we calculated the transport properties of $Ga_{0.51}In_{0.49}P/In_xGa_{1-x}As$/GaAs ($x=0$, 0.15, and 0.25) heterostructures by performing steady-state Monte Carlo simulations at 77 and 300 K for both screened and unscreened cases. Three valleys of the conduction band ($\Gamma$, $L$, and $X$) and band nonparabolicities were included by considering size quantization in the $\Gamma$ valley and the first three subbands in the quantum well. $L$ and $X$ valleys were assumed to have 3D properties. We also treated the electrons with energies larger than the third subband energy as three dimensional. This assumption can be justified due to the closer spacing of the energy levels at high energies which forms a quasicontinuum as in the case of bulk material. The simulation starts by launching the electron in the two-dimensional system. The trajectory of the electron subjected to two-dimensional scattering mechanisms is followed under the applied field, and the electron is placed in the 3D system after it is scattered to the third subband or to the $L$ and $X$ valleys. Once the electron enters the 3D system, it is subjected to 3D scattering mechanisms until it is scattered back to the 2D system. A similar way of two to three dimensional coupling was used by Park and Brennan[20] in their Monte Carlo simulations. However, their approach ignores the third and higher subbands, and places the electron in the 3D system after the electron's energy exceeds the band bending energy. We observed that including the third subband in describing the intersubband scattering processes yields more accurate results. In the quantum well, the scattering mechanisms included in the simulation are polar optical phonon scattering, acoustic phonon scattering, and intervalley (equivalent and nonequivalent) scattering. Self-consistently calculated electronic states were used in the calculation of the 2D scattering rates. We ignored the impurity scattering in the quantum well, since the channel is not considerably doped. The scattering rates for 3D electrons are the same as those given by Fawcett *et al.*[27]

Velocity-field characteristics for $Ga_{0.51}In_{0.49}P/In_xGa_{1-x}As$/GaAs modulation doped heterostructures with different channel In mole fractions ($x$) are shown in Fig. 4. The barrier layer donor doping in the structures is $2\times10^{18}\,\mathrm{cm}^{-3}$ and InGaAs layer thickness is 10 nm in the pseudomorphic structures. The critical field is significantly shifted to lower values at both 77 and 300 K in the screened case. This shift is mainly due to the lower rate of intrasubband scattering in the screened case which results in a lower energy relaxation rate by POP emission. Therefore, in the screened case electrons gain energy from the field at a higher rate and are transferred to lower mobility valleys at relatively low electric fields. Under large fields the difference between the screened and unscreened cases diminishes, since most of the electrons are transferred to 3D-like bands and are subjected to 3D scattering mechanisms for which the screening effects are ignored.

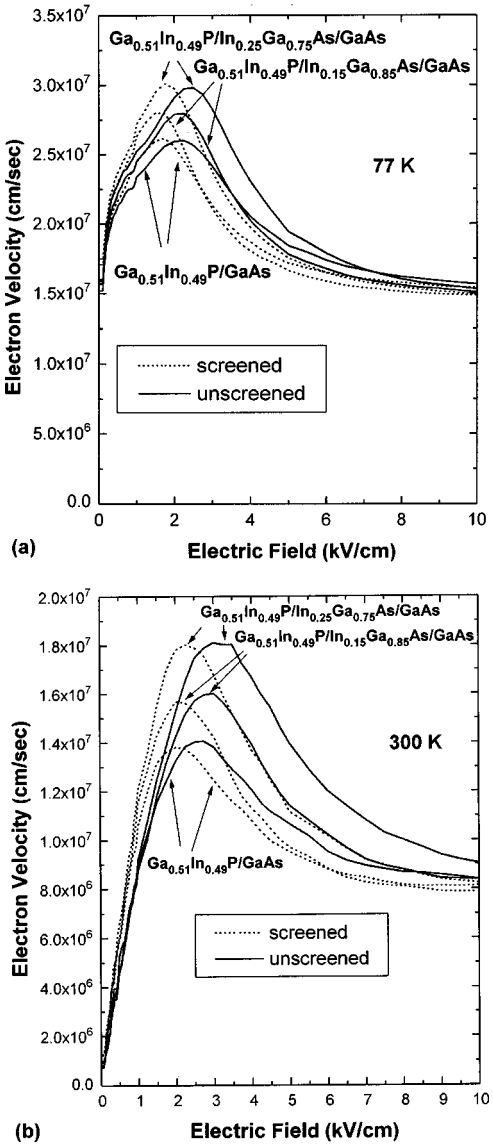


FIG. 4. 77 K (a) and 300 K (b) velocity-field characteristics of lattice matched and pseudomorphic heterostructures. InGaAs layer thickness is 10 nm in the pseudomorphic structures.

Figure 5 presents the band populations at 77 K for the $Ga_{0.51}In_{0.49}P/In_{0.15}Ga_{0.85}As$/GaAs structure in the field range of 1–5 kV/cm. While subband 1 population is lower in the screened case, screening increases the populations of other bands. The decrease in the population of subband 1 with screening is due to a more rapid transfer of electrons from subband 1 to subband 2 and to satellite valleys. The intrasubband POP scattering rates in subband 2 are also decreased with screening resulting in a lower energy relaxation rate in this subband by POP emission. However, screening increases the occupancy of this band due to higher electron transfer

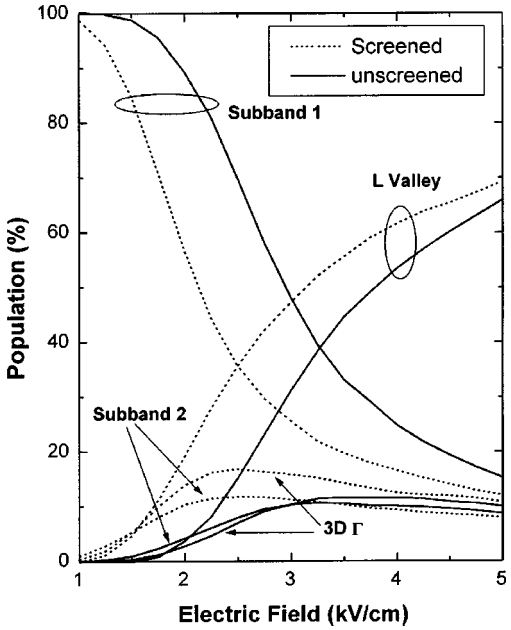


FIG. 5. 77 K band populations vs electric field in the $Ga_{0.51}In_{0.49}P/In_{0.15}Ga_{0.85}As/GaAs$ structure with a barrier layer doping of $2\times10^{18}\,cm^{-3}$ and InGaAs thickness of 10 nm.

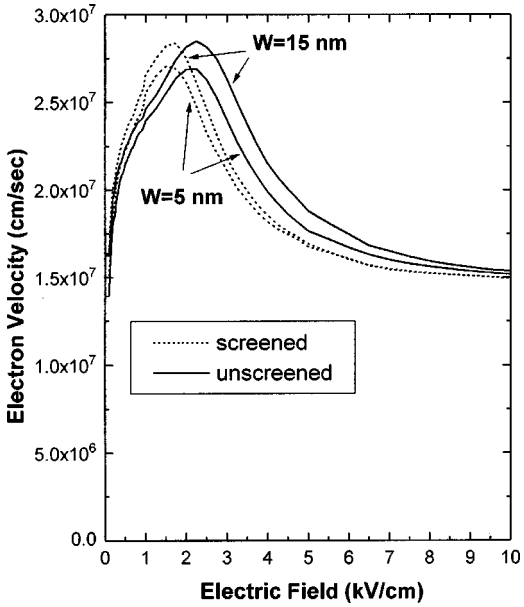


FIG. 6. 77 K velocity-field characteristics for $Ga_{0.51}In_{0.49}P/In_{0.15}Ga_{0.85}As/GaAs$ structures with two different InGaAs layer thicknesses ($W$). Barrier layer doping is $2\times10^{18}\,cm^{-3}$ in both structures.

rate to this subband from subband 1. The maximum 3D-Γ band occupancy is below 20% showing that significant intervalley transfer starts when the electron energy in the quantized system is large enough to populate the third subband. Therefore, taking only the lowest two subbands into account and treating the electron as a 3D electron once it is scattered to the third subband is a reasonable approach in the Monte Carlo analysis of GaAs based quantum well devices.

Velocity-field characteristics for $Ga_{0.51}In_{0.49}P/In_{0.15}Ga_{0.85}As/GaAs$ structures with two different InGaAs layer thicknesses ($W$) of 5 and 15 nm are shown in Fig. 6. The structure with the 15 nm thick InGaAs layer yields better transport properties for both screened and unscreened cases, however the improvement of transport with increasing channel thickness is less apparent in the screened case. It has also been observed that screening modifies the dependence of the transport properties on the 2D electron density in the channel. The above observations clearly show that screening considerably affects the steady-state transport characteristics of the 2D electron gas in modulation doped heterostructures at both 77 and 300 K.

## V. HEMT SIMULATIONS

In order to see the effects of POP screening on HEMT performance, we performed ensemble HEMT Monte Carlo simulations under both screened and unscreened conditions. The simulated device structure is shown in Fig. 7. The simulation is started with $5\times10^4$ electrons distributed throughout the device based on the doping profile. In order to obtain the two-dimensional potential profile in the device, Poisson's equation is solved calculating the total charge in each cell by the cloud in cell method.[28] The time interval for the solution of the equation is selected so that an electron is not allowed to drift through more than one mesh during the interval. The charge neutrality in the source and drain contacts are preserved by injecting new electrons or removing the excess electrons. When the steady state is reached, the number of electrons entering the device becomes equal to the number of electrons leaving the device. The electrons which hit the surfaces are reflected and their wave vectors and positions are changed accordingly. Two to three dimensional coupling is as described in Sec. IV for steady-state transport calculations. Real space transfer is taken into account in the simulation.

The average electron velocity in the quantum well (averaged over the quantum well meshes) under the gate is shown in Fig. 8(a) for a drain-source voltage of 2 V and a gate-source voltage of $-1.5$ V. Figure 8(b) shows the band occupancy in the region covering half of the gate at the drain side. Screening effects are important in both low and high

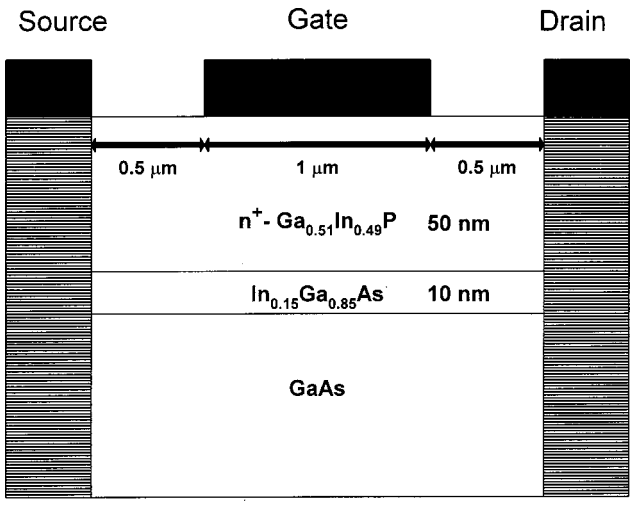


FIG. 7. Simulated device structure.

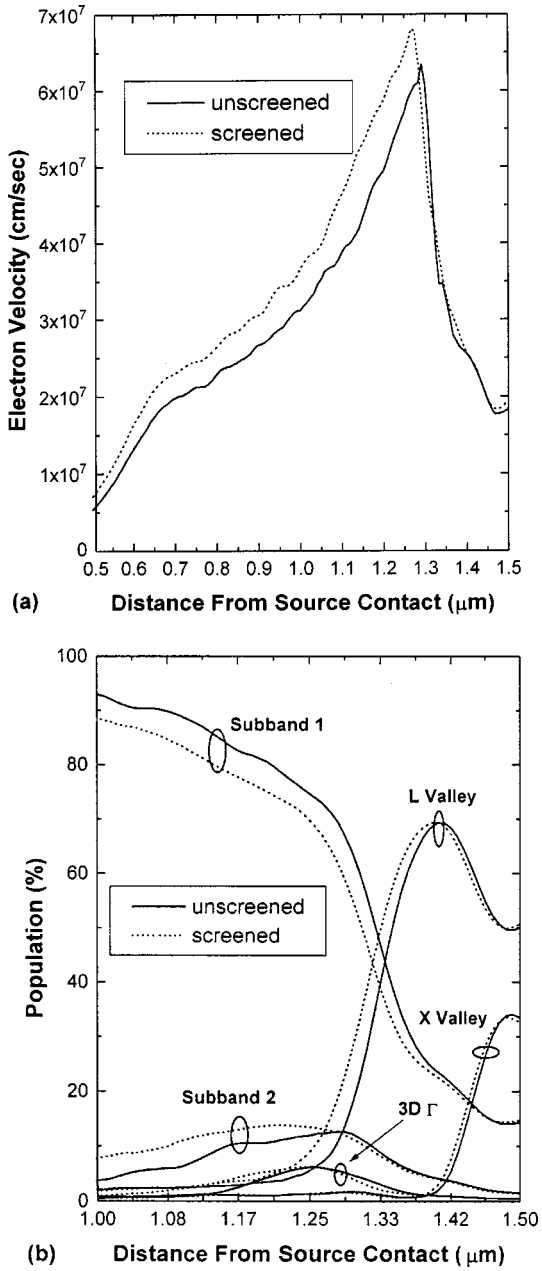


FIG. 8. (a) Average electron velocity in the quantum well under the gate for a drain-source voltage of 2 V and a gate-source voltage of $-1.5$ V. The velocity is averaged over the meshes in the quantum well. (b) Band occupancy in the region covering half of the gate at the drain side.

field regions of the device. In the screened case, the average velocity is considerably larger in a region almost completely covering the gate. In the low field regions, electrons mostly populate subband 1 and subband 2 where they are subjected to 2D scattering. Larger velocity in the screened case in low field regions is due to the larger low field mobility arising from lower intrasubband POP scattering rates. On the other hand, in the high field regions of the device near the drain side, electrons face strong electric field gradients and transfer to the $L$ and $X$ valleys starts. This transfer takes place slightly sooner in the screened case due to the higher energy of the electrons resulting from lower energy relaxation with POP emission. Higher peak velocity in the screened case is mainly due to the higher mobility of the electrons at the location they face the strong field gradient near the drain side. Due to the stronger velocity overshoot in the screened case, screening effects are also important for accurate prediction of the high frequency performance of submicron devices through Monte Carlo simulations. The average electron velocities under the gate are around $3.3\times10^7$ and $2.9\times10^7$ cm/s in screened and unscreened cases, respectively. Therefore, an error of approximately 15% is introduced in the calculation of average electron velocity along the device, if screening effects are ignored. The error introduced by ignoring the screening effects results in a considerable underestimation of both dc and high frequency performance of the device.

## VI. CONCLUSION

The results presented above clearly show that screening is an important factor that needs to be taken into account in Monte Carlo simulations of quantum-well devices such as HEMTs. The reduction in the intrasubband POP scattering rates due to screening significantly affects the transport properties of the heterostructure by decreasing the energy relaxation rate of the two-dimensional electrons. This results in considerable error in the prediction of device performance through the simulation. Another important conclusion of this work is that screening should also be taken into account in the optimization of quantum well structures for better transport characteristics and device performance, since this effect may modify the dependence of transport properties on the quantum well parameters.

## ACKNOWLEDGMENTS

This work is partially supported by the Scientific and Technical Research Council of Turkey under Grants No. EEEAG-168 and No. TBAG-1662, and by NATO (SfP97 1970).

[1] C. Besikci and M. Razeghi, IEEE Trans. Electron Devices **41**, 1066 (1994).
[2] Y. J. Chan, D. Pavlidis, M. Razeghi, and F. Omnes, IEEE Trans. Electron Devices **37**, 2141 (1990).
[3] C. Besikci, Y. Civan, S. Ozder, O. Sen, C. Jelen, S. Slivken, and M. Razeghi, Semicond. Sci. Technol. **12**, 1472 (1997).
[4] C. Besikci and Y. Civan, Thin Solid Films **338**, 213 (1999).
[5] M. Takikawa, T. Ohori, M. Takechi, M. Suzuki, and J. Komeno, J. Cryst. Growth **107**, 942 (1991).
[6] B. Pereiaslevats, G. H. Martin, L. F. Eastman, R. W. Yanka, J. M. Ballingall, J. Braunstein, K. H. Bachem, and B. K. Ridley, IEEE Trans. Electron Devices **44**, 1341 (1997).
[7] B. K. Ridley, J. Phys. C **15**, 5899 (1982).
[8] P. J. Price, Ann. Phys. **133**, 217 (1981).
[9] P. J. Price, Surf. Sci. **113**, 199 (1982).
[10] K. Hess, Appl. Phys. Lett. **35**, 484 (1979).
[11] K. Yokoyama and K. Hess, Phys. Rev. B **33**, 5595 (1986).
[12] P. K. Basu and B. R. Nag, Appl. Phys. Lett. **43**, 689 (1983).
[13] M. Tomizawa, K. Yokoyama, and A. Yoshii, IEEE Electron Device Lett. **5**, 464 (1984).
[14] K. S. Yoon, G. B. Stringfellow, and R. J. Huber, J. Appl. Phys. **62**, 1931 (1987).
[15] K. S. Yoon, G. B. Stringfellow, and R. J. Huber, J. Appl. Phys. **63**, 1126 (1988).
[16] O. Sen, C. Besikci, and B. Tanatar, Solid-State Electron. **42**, 987 (1998).
[17] G. Salmer, J. Zimmerman, and R. Fauquembergue, IEEE Trans. Microwave Theory Tech. **36**, 1124 (1988).

[18] K. Tomizawa and N. Hashizume, IEEE Trans. Electron Devices **35**, 849 (1988).
[19] U. Ravaioli and D. K. Ferry, IEEE Trans. Electron Devices **33**, 677 (1986).
[20] D. H. Park and K. F. Brennan, IEEE Trans. Electron Devices **36**, 1254 (1989).
[21] P. J. Price, J. Vac. Sci. Technol. **19**, 599 (1981).
[22] P. K. Basu and S. Kundu, Appl. Phys. Lett. **47**, 264 (1985).
[23] P. C. Chow, Am. J. Phys. **40**, 730 (1972).
[24] F. Stern and S. Das Sarma, Phys. Rev. B **30**, 840 (1984).
[25] P. Sotirelis, P. von Allmen, and K. Hess, Phys. Rev. B **47**, 12744 (1993).
[26] S. Mori and T. Ando, Phys. Rev. B **19**, 6433 (1979).
[27] W. Fawcett, A. D. Boardman, and S. Swain, J. Phys. C **31**, 1963 (1970).
[28] R. W Hockney and J. W. Eastwood, *Computer Simulation Using Particles* (Hilger, New York, 1988).